

# An Empirical Study on the Effects of Translucency on Photometric Stereo

Kathleen D. Moore · Pieter Peers

**Abstract** We present an empirical study on the effects of translucency on photometric stereo. Our study shows that the impact on the accuracy of the photometric normals is related to the relative size of the geometrical features and the mean free path. We show that under simplified conditions, the obtained photometric normals are a blurred version of the true surface normals, where the blur kernel is directly related to the subsurface scattering profile. We furthermore investigate the impact of scattering albedo, index of refraction, and single scattering on the accuracy. We perform our analysis using simulations, and demonstrate the validity on a real world example.

**Keywords** Subsurface Scattering · Photometric Stereo

## 1 Introduction

Digitally reproducing the appearance of physical objects is a difficult and important problem in computer graphics and computer vision. Both shape and reflectance need to be accurately characterized in order to obtain a faithful reproduction. While modern geometry acquisition techniques are capable of achieving sub-millimeter accurate results [12], these methods make no guarantees on the accuracy of the resulting surface normal. However, accurate surface normals are important to faithfully reproduce surface reflectance. A practical solution is to directly acquire surface normals that are

then subsequently used to augment the high resolution geometry [18].

Photometric stereo [21] is a lightweight and versatile method for direct acquisition of surface normals. The original formulation of photometric stereo is only strictly valid for unoccluded Lambertian surfaces, and has been extended and generalized to handle, amongst others, shadowing, specularities, and general surface reflectance. However, a key assumption that underlies all photometric stereo variants is that the reflected radiance is directly proportional to the incident irradiance at each surface point.

The appearance of translucent materials, such as milk, skin, marble, etc., is characterized by the subsurface transport of incident lighting. Due to the multiple subsurface scattering events that incident lighting undergo, the directional dependence to the incident lighting is lost [20]. This apparent diffuse reflectance behavior seems to indicate that translucent materials are ideally suited for traditional photometric stereo. However, the incident irradiance at a surface point can contribute to the exitant radiance at potentially many other surface points, breaking the critical assumption that incident and exitant radiance at a surface point are tightly coupled.

In this paper, we perform an empirical study to investigate the impact of violating the coupling of incident and exitant radiance assumption on the accuracy of photometric stereo on translucent materials. We perform simulations based on Jensen et al.'s [14] dipole-diffusion model and compute the accuracy of photometric stereo as a function of mean free path, scattering albedo, mean cosine of the phase function, and number of light source directions. Our analysis shows that the ratio of geometric feature size versus mean free path and single scattering play an important role, whereas the

---

Kathleen D. Moore  
College of William & Mary, Williamsburg, VA, USA  
E-mail: kdm@cs.wm.edu

Pieter Peers  
College of William & Mary, Williamsburg, VA, USA

other parameters influence the error less. We demonstrate the validity of our analysis on a physical material sample.

To the best of our knowledge, the relation between the coupling of incident and exitant radiance has not yet been explored in the context of photometric stereo. With the ever increasing drive for higher resolution geometry, understanding this relation and its impact on the accuracy of photometric stereo becomes critical as materials that at low or moderate resolution appear diffuse, can exhibit subsurface light transport when examined at a finer resolution.

## 2 Related Work

**Photometric Stereo.** Photometric stereo, first introduced by Woodham [21], is a convenient and lightweight technique for estimating surface normals of unoccluded Lambertian objects, from as little as three observations under different directional light sources. Computing the surface normal of a pixel involves solving a linear system:  $O = NL$ , where  $O$  is a  $1 \times 3$  vector of observed radiance values under the three light source directions  $L = [L_1, L_2, L_3]$  (a  $3 \times 3$  matrix), and  $N$ , a  $1 \times 3$  vector, is the unknown *unnormalized* surface normal. Photometric stereo is only strictly valid for unoccluded Lambertian objects under known directional lighting. Since its inception, several variants have been proposed that extend photometric stereo to handle more general lighting conditions (e.g., [16,3]), shadows (e.g., [2]), non-Lambertian reflectance (e.g., [9,1]), etc. Ma et al. [15] propose to employ spherical gradient illumination to estimate photometric normals, and observe that there is a discrepancy between so-called “diffuse” and “specular” normals and speculate that this is due to interreflections and subsurface scattering. None of the above has analyzed the impact of the different parameters of subsurface scattering on the accuracy of photometric stereo.

**Subsurface Scattering.** Light transport in a translucent material is characterized by the 8 dimensional Bidirectional Subsurface Scattering Reflectance Distribution Function (BSSRDF) [19]. However, simulating subsurface light transport directly using the 8D BSSRDF is computationally expensive. For optically dense materials, Stam [20] noted that light transport can be accurately approximated by a diffusion process. Jensen et al. [14] introduced the dipole-diffusion approximation, an analytical solution for the diffusion process in a planar, semi-infinite slab of a homogeneous translucent material. Donner and Jensen [5] extended this model to multi-layer translucent materials. Recently, d’Eon and Irving [4] introduced the quantized diffusion model that

more accurately approximates subsurface light transport for a wider range of translucent materials. The above papers focus mainly on image-synthesis. We will employ the dipole-diffusion approximation to predict the impact of translucency on photometric stereo.

**Shape Acquisition of Translucent Objects.** Acquiring the shape of a translucent object is a challenging problem. Godin et al. [7] study the optical properties of marble under laser range scanning, and observe a significant bias in depth measurement. To avoid such bias, Goesele et al. [8] resort to “dusting” the translucent object, effectively eliminating subsurface scattering, to obtain more accurate shape estimates. Nayar et al. [17] propose a novel method to separate direct reflection from subsurface scattered reflected illumination using multiple high-frequency sinusoidal illumination patterns. Holroyd and Lawrence [11] formally analyze the applicability and expected error of using this separation technique on optical triangulation methods. Recently, Inoshita et al. [13] reconstruct the shape of a translucent object by only looking at the single scattering component. Finally, Ma et al. [15] compute photometric normals from the direct surface reflection of translucent materials under spherical gradient illumination. They exploit the fact that multiple scattering tends to depolarize incident lighting, and rely on polarization difference imaging to separate subsurface from surface reflections. While they observe that the “diffuse” photometric normals are significantly less sharp, they do not formally analyze the error with respect to scattering parameters.

## 3 Empirical Study

To study the effects of translucency on the accuracy of photometric stereo, we simulate subsurface light transport in a simplified setting. This allows us to carefully control all the relevant parameters and study the influence of each of the parameters separately.

**Background.** In our simulation we consider a homogeneous optically dense translucent material, and model the 8D BSSRDF [19] over incident position  $x_i$ , outgoing position  $x_o$ , incident direction  $\omega_i$  and outgoing direction  $\omega_o$  as the sum of a single scattering and a multiple scattering term:

$$S(x_i, \omega_i; x_o, \omega_o) = S^1(x_i, \omega_i; x_o, \omega_o) + S^d(x_i, \omega_i; x_o, \omega_o). \quad (1)$$

Multiple scattering  $S^d(x_i, \omega_i; x_o, \omega_o)$  can be further refined as:

$$\frac{1}{\pi} F_t((\omega_i \cdot n_{x_i}), \eta) R_d(\|x_i - x_o\|) F_t((\omega_o \cdot n_{x_o}), \eta), \quad (2)$$

where  $n_x$  is the surface normal at position  $x$ ,  $R_d(\|x_i - x_o\|)$  is the diffuse reflectance describing the subsurface transport from point  $x_i$  to  $x_o$ , and  $F_t$  is the Fresnel transmission term with index of refraction  $\eta$ . In our analysis we employ the dipole-diffusion approximation for  $R_d$  [14]. However, our analysis is not specific to the the dipole-diffusion model, and other models, such as the quantized diffusion model [4], can also be used.

Finally, we employ the BRDF approximation of Hanrahan and Krueger [10] for the single scattering  $S^1$  term:

$$f_r^{-1}(x, \omega_i, \omega_o) = \alpha F \frac{p(g, \omega_i' \cdot \omega_o')}{|(n_{x_o} \cdot \omega_i')| + |(n_{x_o} \cdot \omega_o')|}, \quad (3)$$

where  $\alpha$  is the scattering albedo,  $F$  the product of the incident and exitant transmission terms  $F_t$ ,  $p(g, \omega_i' \cdot \omega_o')$  is the phase function in terms of the mean cosine  $g \in [-1, +1]$ , and the refracted incident and outgoing directions  $\omega_i'$  and  $\omega_o'$  respectively.

We ignore surface reflectance and assume directional (i.e., distant lighting). Furthermore, we only consider subsurface light transport and ignore interreflections.

**Setup.** Our simulation setup consists of an orthographic camera looking down (along the Z axis) onto a planar homogeneous sample of  $10cm^2$ . The sample only exhibits sinusoidal surface depth variation (with a wavelength of  $1cm$  and an amplitude of  $\frac{\pi}{2}cm$ ) along the X axis, while remaining constant along the Y axis, as shown in Figure 1. The surface sample is illuminated by a variable number of light sources equally distributed in a  $40^\circ$  cone around the view direction, ensuring that foreshortening is non-zero (i.e.,  $(n_{x_i} \cdot \omega_i) \leq 0$ ) for any surface point  $x_i$  and directional lighting direction  $\omega_i$ . Unless noted, we employ three directional light sources in our simulations.

For each lighting direction, the outgoing radiance is computed for every surface point  $x_o$  at a resolution of  $500 \times 500$  (a pixel to  $mm$  ratio of 0.2), and fed into a least squares photometric stereo algorithm. For each estimated photometric surface normal  $\hat{n}_{x_o}$ , the error with the ground truth normal  $n_{x_o}$  is computed as the angle between the estimated and ground truth normal expressed in radians:  $|\arccos(\hat{n}_{x_o} \cdot n_{x_o})|$ .

**Multiple Scattering.** For our first experiment we only consider multiple scattering, and set  $\eta = 1.0$  (i.e.,  $F_t = 1$ ), and  $g = 0$ . In this case the outgoing radiance  $L(x_o, \omega_o)$  becomes:

$$\begin{aligned} L(x_o, \omega_o) &= \frac{1}{\pi} \int_A R_d(\|x_i - x_o\|)(\omega_i \cdot n_{x_i}) dx_i, \\ &= \frac{1}{\pi} (\omega_i \cdot \int_A R_d(\|x_i - x_o\|) n_{x_i} dx_i), \\ &= \frac{\gamma_{x_o}}{\pi} (\hat{n}_{x_o} \cdot \omega_i). \end{aligned} \quad (4)$$

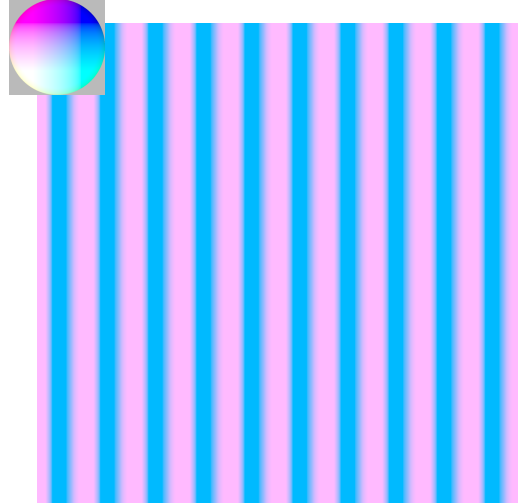


**Fig. 1** The ground truth normal map employed in our simulations. The sample size is  $10cm^2$ , and the amplitude of the sinusoidal normal variation is  $\frac{\pi}{2}cm$ . The inset shows the false-color coding of the normals.

where  $\gamma_{x_o}$  is a spatially varying scalar scale factor,  $\hat{n}_{x_o}$  is the normalized blurred surface normal that is the result of the sum of the surface normals around  $x_o$  weighted by the diffuse reflectance  $R_d$ . An alternative interpretation is that the blurred normal is proportional to the convolution of the normal field with the diffuse reflectance:  $\hat{n}_{x_o} \sim (n * R_d)_{x_o}$ .

Note that Equation (4) matches the Lambertian reflectance model, where  $\gamma_{x_o}$  plays the role of a spatially varying albedo map, and the blurred normal  $\hat{n}_{x_o}$  acts as surface normal. Consequently, the normal estimated through photometric stereo will be the blurred surface normal  $\hat{n}_{x_o}$ .

From this analysis it follows that the accuracy of photometric stereo on a translucent material (only exhibiting multiple scattering and with an index of refraction of 1.0), depends on the shape of the diffuse reflectance  $R_d$ . If  $R_d$  is a delta function (and thus no subsurface scattering occurs), then the blurred normal  $\hat{n}$  will exactly match the ground truth normal  $n$ . To better understand the impact of the shape of the diffuse reflectance  $R_d$ , we plot (Figure 2) the average error on the setup described above for a dense sampling of scattering albedo  $\alpha$  (vertical axis ranging from 0.1 to 1.0) and mean free path  $l_d$  (horizontal axis ranging from 0.35 to 6.5)<sup>1</sup>.

From Figure 2 it can be seen that the average error increases with increasing  $l_d$  – increasing mean free path implies a more translucent material. Indeed, at the ex-

<sup>1</sup> Scattering albedo is defined as:  $\alpha = \frac{\sigma_s}{\sigma_s + \sigma_a}$ ; the ratio of scattering over scattering+absorption. Mean free path is defined as:  $l_d = \frac{1}{\sigma_s + \sigma_a}$ .

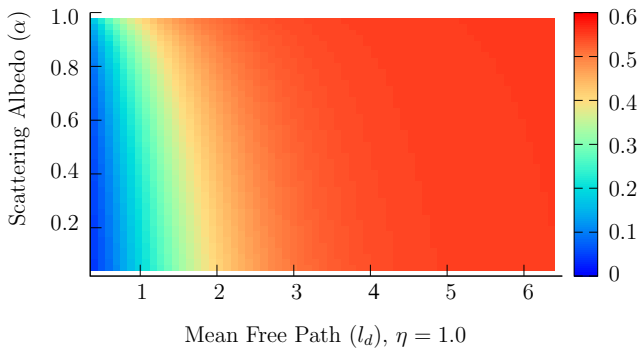


**Fig. 2** The average angular error plot for photometric normals computed from observations under three directional light sources, and for multiple scattering only, without taking Fresnel transmittance into account (i.e.,  $\eta = 1.0$ ) for scattering albedo  $\alpha \in [0.1, 1.0]$  and mean free path  $l_d \in [0.35, 6.5]$ .

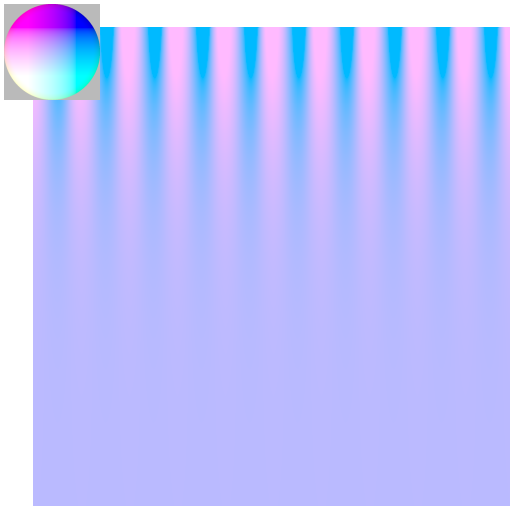


**Fig. 3** The impact of varying mean free path (vertical axis) on a slice from the normal map. As mean free path increases, the features in the normal map gradually become blurred out.

trême right, the extent of the diffuse reflectance profile significantly exceeds the wavelength of the sinusoid, and all normal variation is essentially blurred away. This is illustrated in Figure 3 where we repeat a single line (horizontal) from the recovered normal map for a fixed  $\alpha = 0.8$  and increasing  $l_d$  (vertical). Note that changing the wavelength of the sinusoidal surface variation, is equivalent to scaling mean free path inversely by the same scale factor [6]. Thus, changing the relative size of the geometric features results in a similar average error plot but scaled along the Y-axis.

**Effect of Index of Refraction.** The previous analysis employs an index of refraction of 1.0 which is not very realistic. If we allow the index of refraction to take on other values than 1 (i.e.,  $F_t \neq 1$ ), then we can make two observations. First, the exitant Fresnel transmittance term is independent of  $x_i$  and thus does not impact the integral over the irradiance. Second, for

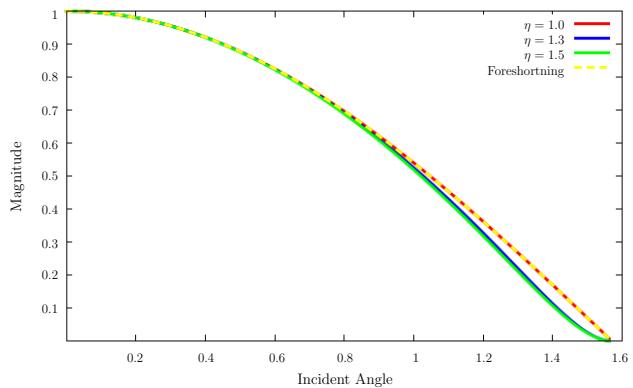


**Fig. 4** A comparison of  $\frac{F_t(\omega_{iz}, \eta)\omega_{iz}}{F_{t0}}$  for varying indices of refraction.

plausible indices of refraction,  $F_t$  remains fairly constant over a large portion of its domain, varying only significantly towards grazing angle. However, towards grazing angle the foreshortening goes to zero, limiting the impact of the drop in Fresnel transmittance. Therefore, we can approximate  $F_t((\omega_i \cdot n_{x_i}), \eta)(n_{x_i} \cdot \omega_i)$  by  $F_{t0} \times (n_{x_i} \cdot \omega_i)$ , where the scalar  $F_{t0}$  is the transmittance at normal incidence (Figure 4). Thus, Equation (4) can be rewritten as:

$$\begin{aligned} L(x_o, \omega_o) &= \frac{1}{\pi} \int_A F_t((\omega_o \cdot n_{x_o}), \eta) R_d(\|x_i - x_o\|) \\ &\quad F_t((\omega_i \cdot n_{x_i}), \eta)(\omega_i \cdot n_{x_i}) dx_i, \\ &\approx \frac{F_{t0} F_t((\omega_o \cdot n_{x_o}), \eta)}{\pi} \\ &\quad (\omega_i \cdot \int_A R_d(\|x_i - x_o\|) n_{x_i} dx_i), \\ &= \frac{\gamma_{x_o}}{\pi} (\hat{n}_{x_o} \cdot \omega_i), \end{aligned} \quad (5)$$

where the Fresnel transmittance terms are absorbed in the scale factor  $\gamma_{x_o}$ , yielding a similar expression as before. Note that the diffuse reflectance  $R_d$  changes slightly in shape as index of refraction changes.

Figure 5 shows the average error for indices of refraction of 1.1, 1.3 and 1.5. As predicted, the difference with the average error plot (with index of refraction of 1.0) shown in Figure 2 is minimal.

**Single Scattering.** Single scattering is often approximated as a BRDF. Therefore, it does not break the assumption that incident irradiance is tightly coupled to exitant radiance. While not exactly Lambertian, depending on the mean cosine  $g$ , single scattering can have an approximate Lambertian behavior for a large range of incident directions.

Due to the linearity of light transport, the observed radiance from a translucent material can be written as the sum of the exitant radiance due to single scattering  $L^1$  and the exitant radiance due to multiple scattering

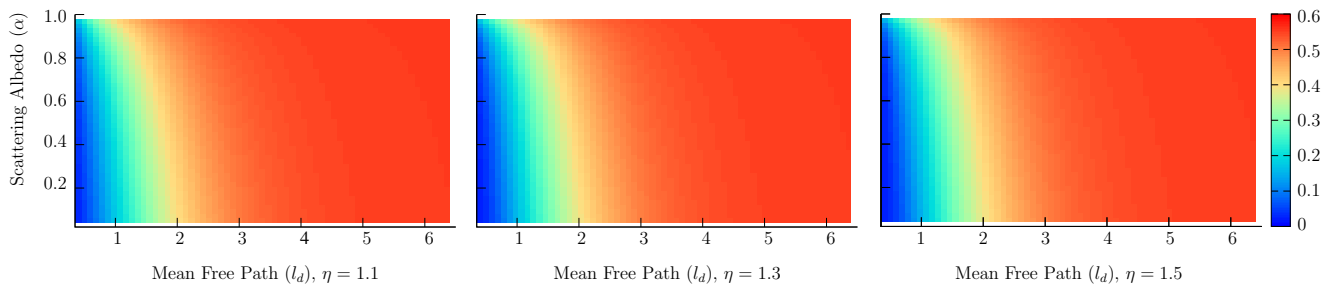


**Fig. 5** The average angular error plot for photometric normals computed from observations under three directional light sources, and for multiple scattering only, with varying index of refraction  $\eta \in \{1.1, 1.3, 1.5\}$ , for scattering albedo  $\alpha \in [0.1, 1.0]$  and mean free path  $l_d \in [0.35, 6.5]$ .

$L^d$ :

$$L(x_o, \omega_o) = L^1(x_o, \omega_o) + L^d(x_o, \omega_o). \quad (6)$$

However, since photometric stereo is a linear process too, the resulting normal is also a linear combination of the blurred multiple scattering normal  $\hat{n}^d$ , and the single scattering normal  $\hat{n}^1$ :

$$\hat{n}_{x_o} = \frac{\gamma_1 \hat{n}_{x_o}^1 + \gamma_d \hat{n}_{x_o}^d}{|\gamma_1 \hat{n}_{x_o}^1 + \gamma_d \hat{n}_{x_o}^d|}. \quad (7)$$

The relative contribution of single scattering to the resulting estimated photometric normal depends on the normalization constants  $\gamma_d$  and  $\gamma_1$ , which in turn depend on the mean cosine  $g$ . Figure 6 shows error plots for  $g = -0.5, 0.0, +0.5$ . We observe that, while the accuracy improves for all cases, the impact of backscattering (i.e.,  $g < 0$ ) is stronger than of isotropic scattering ( $g = 0$ ), which in turn is stronger than forward scattering. However, for  $|g| \rightarrow 1$ , the reflectance behavior is significantly non-Lambertian, at which point the presence of single scattering negatively impacts the accuracy of the estimated normals.

**Lighting Directions.** As a final experiment, we increased the number of light source from three to four, and solve for the photometric normal in a least squares sense. Using more than three light sources can often help in improving the photometric normal estimate. Figure 7 shows the average error plot for multiple scattering ( $\eta = 1.3$ ). Due to the diffusion of exitant radiance, increasing the number of light source does not provide additional information, and the obtained photometric normals are identical. From this it can be concluded that increasing the number of light source directions, will not yield a significant improvement in accuracy.

**Physical Validation.** We show the validity of our analysis by capturing the photometric normals of a translucent soap sample. We estimate both the normals from multiple scattering only, and from the full subsurface scattering light transport (i.e., single scattering and

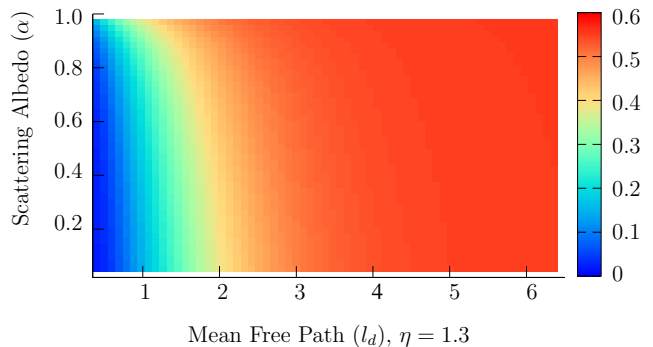


**Fig. 7** The average angular error plot for photometric normals computed from observations under four directional light sources, and for multiple scattering only, with  $\eta = 1.3$ , scattering albedo  $\alpha \in [0.1, 1.0]$  and mean free path  $l_d \in [0.35, 6.5]$ .

multiple scattering). Our setup consists of a DSLR camera located approximately 1.5m away from the subject, and four flash light sources placed around the camera aimed at the sample. We place a linear polarizer in front of the camera, and to the light sources. We tune the linear polarizers on the light sources such that specular reflections from a dielectric ball are canceled out (i.e., cross polarized). We calibrate the light directions and intensities of the individual flash lights using a Spectralon sphere. Next, we capture two pairs of four photographs, one pair cross polarized  $I_i^0$ , and one pair  $I_i^{90}$  where we rotate the linear polarizer on the camera by 90 degrees. The images  $I_i^0$  will only display (half of) multiple scattered light, and  $I_i^{90}$  contains all reflected components: (half of) multiple scattering, (full) single scattering, and is potentially polluted by specular surface reflectance. The sum of both  $I_i = I_i^0 + I_i^{90}$  is equivalent to a photograph without a polarization filter in front of the camera.

Figure 8 shows (on the right from top to bottom)  $2I_i^0$ ,  $I_i - 2I_i^0$ , and  $I_i$  for a single lighting direction. The difference image shows the amount of single scattering that was canceled out in  $I_i^0$ . Note, that this difference also clearly contains some specular ‘‘pollution’’, which will affect the photometric results. Figure 8 (right) shows

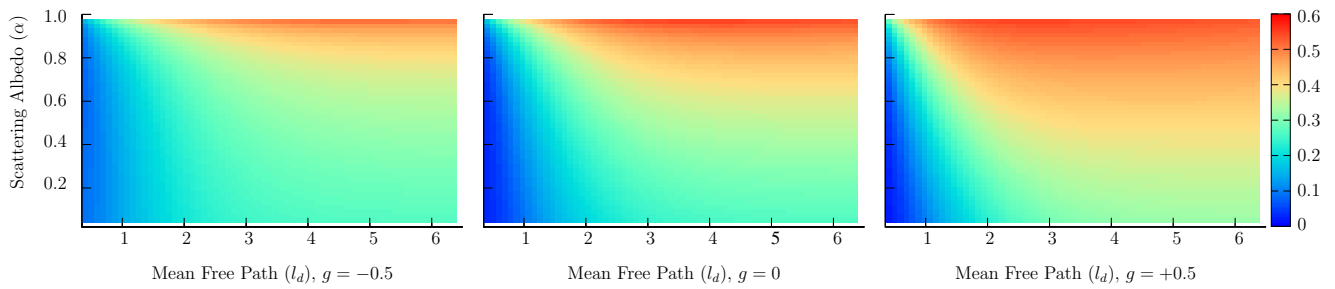


**Fig. 6** The average angular error plot for photometric normals computed from observations under three directional light sources, and for multiple scattering and single scattering (i.e.,  $\eta = 1.3$ ) with the mean cosine  $g \in \{-0.5, 0.0, +0.5\}$ , for scattering albedo  $\alpha \in [0.1, 1.0]$  and mean free path  $l_d \in [0.35, 6.5]$ .

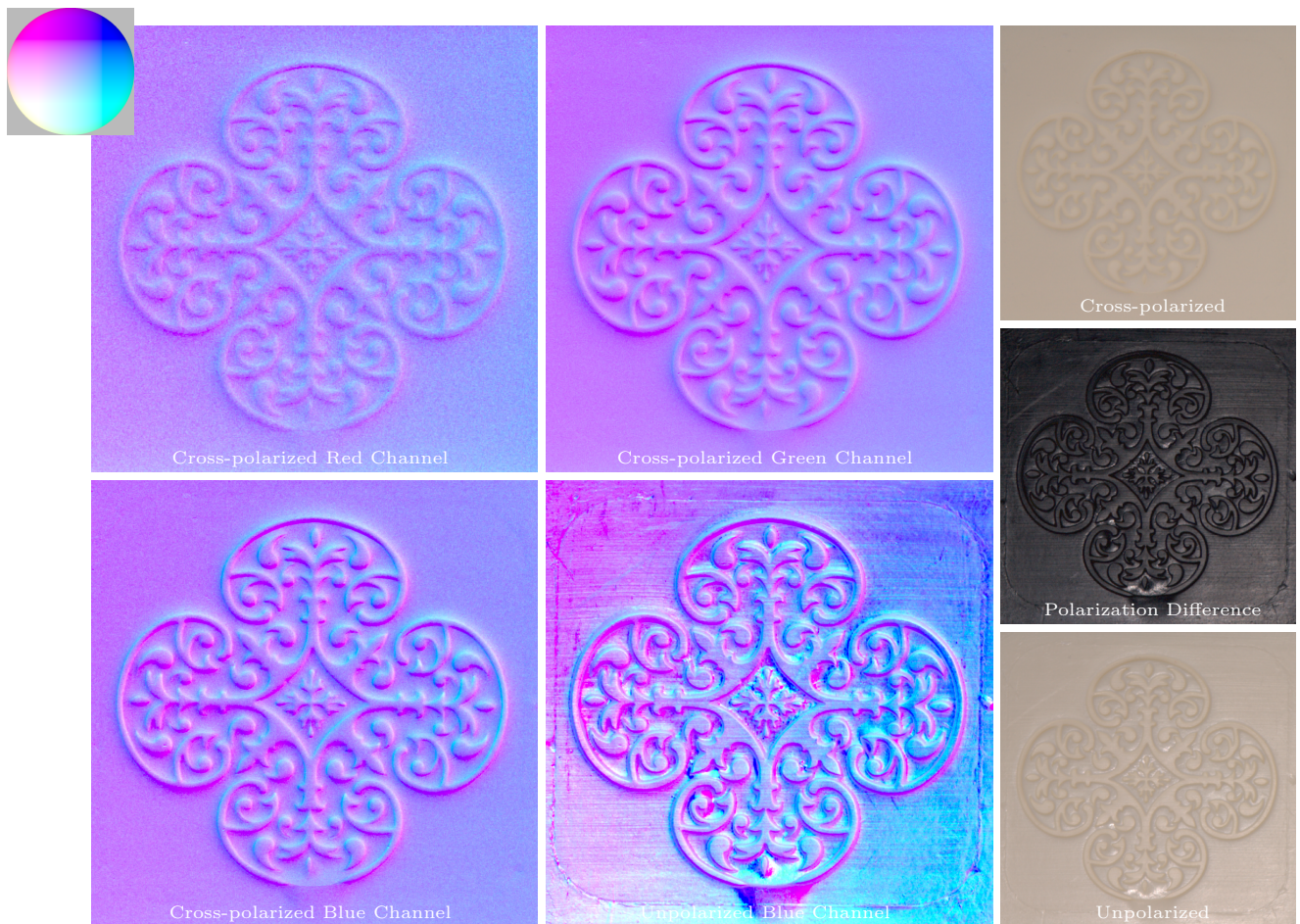


**Fig. 8 Left:** Photometric normals estimated from a translucent soap sample. Note how multiple scattering blurs out most surface details compared to the multiple+single scattering photometric normal map. Further observe the effect of the wavelength dependent diffuse reflectance  $R_d$  on the sharpness of the photometric normals. **Right-top:** a cross-polarized captured image, exhibiting only multiple subsurface scattering, used to compute the multiple scattering photometric normals. **Right-middle:** polarization difference image showing the specular surface reflectance and single scattering removed by cross polarization. **Right-bottom:** unpolarized photograph of the translucent soap, showing both reflectance due to multiple as well as single scattering.

the resulting photometric normals computed from  $I_i^0$  (computed separately for the red, green and blue color channels) and the photometric surface normals computed from the blue color channel of  $I_i$ .

As predicted by our analysis, it can be clearly seen that the photometric normals computed from only multiple scattering exhibits very little surface detail. Since mean free path and scattering albedo are wavelength dependent, the “blur” kernel  $R_d$  differs. Consequently, the photometric surface normals for the different color channels differ slightly, resulting in blurrier normals for the red color channel, and the sharpest normals for blue. This illustrates, that indeed as predicted, an increase in mean free path yields more blurred surface normals, and thus less surface details. While the photometric normals computed from  $I_i$  are biased due to specular surface reflection, it can be seen how much surface detail is lost by only considering multiple scattering.

## 4 Conclusions

We have presented an empirical study on the effects of translucency on photometric stereo. We have shown that multiple scattering has a blurring effect on the photometric normals, resulting in a less detailed shape characterization. We have shown that the relative size of mean free path versus geometrical feature size is the primary parameter that determines the accuracy of the results. We have found that index of refraction and scattering albedo have less of an impact on the final error. Although we rely on the dipole-diffusion approximation for our analysis, our analysis well-predicts the types of error that will be encountered when acquiring the surface normals of a physical translucent sample.

Our analysis currently ignores interreflections and specular surface reflections. For future work we would like to include these factors too. Furthermore, we rely on the dipole-diffusion approximation which does not necessarily model translucent materials well for small scattering albedo. Employing a particle simulation to accurately simulate the light transport would yield a more accurate analysis.

To the best of our knowledge, our work is the first to investigate the impact of translucency on the accuracy of photometric stereo. We hope that our work will inspire other researchers to develop new variants of photometric stereo that can yield accurate surface normals for translucent objects.

## Acknowledgments

This work was supported in part by Google, and NSF grants IIS-1016703 and IIS-1217765. The first author acknowledges additional support from the Virginia Space Grant Consortium.

## References

1. N. Alldrin and D. Kriegman. Toward reconstructing surfaces with arbitrary isotropic reflectance: A stratified photometric stereo approach. In *Proc. Int. Conf. Computer Vision*, pages 1–8, 2007.
2. S. Barsky and M. Petrou. The 4-source photometric stereo technique for three-dimensional surfaces in the presence of highlights and shadows. *IEEE Trans. Pattern Anal. Mach. Intell.*, 25(10):1239–1252, 2003.
3. R. Basri and D. Jacobs. Photometric stereo with general, unknown lighting. In *Proc. Conf. Computer Vision and Pattern Recognition*, pages 374–381, 2001.
4. E. D’Eon and G. Irving. A quantized-diffusion model for rendering translucent materials. *ACM Trans. Graph.*, 30(4):56:1–56:14, July 2011.
5. C. Donner and H. W. Jensen. Light diffusion in multi-layered translucent materials. *ACM Trans. Graph.*, 24(3):1032–1039, 2005.
6. C. Donner, J. Lawrence, R. Ramamoorthi, T. Hachisuka, H. W. Jensen, and S. K. Nayar. An empirical bsrdf model. *ACM Trans. Graph.*, 28(3), 2009.
7. G. Godin, J.-A. Beraldin, M. Rioux, M. Levoy, L. Cournoyer, and F. Blais. An assessment of laser range measurement of marble surfaces. In *Proc. Fifth Conference on optical 3-D measurement techniques*, 2001.
8. M. Goesele, H. P. A. Lensch, J. Lang, C. Fuchs, and H.-P. Seidel. Disco: acquisition of translucent objects. *ACM Trans. Graph.*, 23(3):835–844, August 2004.
9. D. B. Goldman, B. Curless, A. Hertzmann, and S. M. Seitz. Shape and spatially-varying brdfs from photometric stereo. In *Proc. Conf. Computer Vision and Pattern Recognition*, pages 341–348, 2005.
10. P. Hanrahan and W. Krueger. Reflection from layered surfaces due to subsurface scattering. In *Proc. SIGGRAPH 93*, pages 165–174, 1993.
11. M. Holroyd and J. Lawrence. An analysis of using high-frequency sinusoidal illumination to measure the 3d shape of translucent objects. In *Proc. Conf. Computer Vision and Pattern Recognition*, pages 2985–2991, 2011.
12. M. Holroyd, J. Lawrence, and T. Zickler. A coaxial optical scanner for synchronous acquisition of 3d geometry and surface reflectance. *ACM Trans. Graph.*, 29(4), 2010.
13. C. Inoshita, Y. Mukaigawa, Y. Matsushita, and Y. Yagi. Shape from single scattering for translucent objects. In *Proc. European Conf. Computer Vision*, pages 371–384, 2012.
14. H. W. Jensen, S.R. Marschner, M. Levoy, and P. Hanrahan. A practical model for subsurface light transport. In *Proc. SIGGRAPH 2001*, pages 511–518, 2001.
15. W. Ma, T. Hawkins, P. Peers, C. Chabert, M. Weiss, and P. Debevec. Rapid acquisition of specular and diffuse normal maps from polarized spherical gradient illumination. In *Proc. Eurographics Symposium on Rendering*, 2007.

16. S. K. Nayar, K. Ikeuchi, and T. Kanade. Determining shape and reflectance of lambertian, specular, and hybrid surfaces using extended sources. In *International Workshop on Industrial Applications of Machine Intelligence and Vision*, pages 169–175, 1989.
17. S. K. Nayar, G. Krishnan, M. D. Grossberg, and R. Raskar. Fast separation of direct and global components of a scene using high frequency illumination. *ACM Trans. on Graphics*, 25(3):935–944, 2006.
18. D. Nehab, S. Rusinkiewicz, J. Davis, and R. Ramamoorthi. Efficiently combining positions and normals for precise 3d geometry. *ACM Trans. on Graphics*, 24(3):536–543, 2005.
19. F. E. Nicodemus, J. C. Richmond, J. J. Hsia, I. W. Ginsberg, and T. Limperis. Geometric considerations and nomenclature for reflectance. *National Bureau of Standards Monograph 160*, 1977.
20. J. Stam. Multiple scattering as a diffusion process. In *Proc. Eurographics Workshop on Rendering*, pages 41–50, 1995.
21. R. J. Woodham. Photometric method for determining surface orientation from multiple images. *Optical Engineering*, 19(1):3050–3068, 1980.